UCPH NanoScience
NanoVidenskab KU

tidsskrift.dk/index.php/NanoVidenskabKU

Report

Synthesis and characterization of $CuCrO_2$ delafossite nanoplatelets through Rietveld refinement and Pair distribution function analysis

Emil Thyge Skaaning Kjær

Received June 2017, Accepted April 2018

Delafossite (ABO_2) nanostructures such as $CuCrO_2$ nanoparticles have shown promising properties in dye-sensitized solar cells (DSSCs). Previous studies have shown that changing the metal on either the A or B site in the structure, influences both the conditions required to synthesize delafossite compounds, their properties, and their tendency of forming nanocrystals or bulk particles. The crystallites can further be doped changing the conductivity further. Here, we present a series of syntheses with varying parameters, illustrating how the conditions must be optimized to obtain the pure delafossite $CuCrO_2$ phase. Structure characterization was done through Powder X-ray Diffraction (PXRD) showing change in crystallite size with increasing synthesis time and temperature. By varying both temperature and time, the amount of secondary phase (CuO) in the final product can be minimized. It was only possible to synthesize pure delafossite when certain criteria regarding pH, temperature and time were met. Rietveld refinement of the PXRD data showed anisotropic nanocrystallites with approximate sizes of 130x130x40Å with the trigonal delafossite unit cell. However, the crystallites are too small and anisotropic to give a satisfying fit using conventional Rietveld refinement, and the sizes were obtained through anisotropic "no rules" model. Pair Distribution Function (PDF) analysis of X-ray total scattering data were used to obtain further understanding of structural disorder in the crystallites.

Introduction

Delafossite crystals have over the last years received a large amount of attention because of their p-type electrical conductivity and low fabrication cost.[1,2] A large diversity of delafossite compositions have been synthesized with different metals on the A and B sites, A = Ag or Cu, B = B, Al, Ga, In, Fe, Cr, Sc, Y, etc. all having high p-type conductivity.[3] Delafossite materials have many different applications, such as in transparent conducting oxides, luminescent materials, catalysts, batteries, ferroelectrics, etc.[4] Especially $CuAlO_2$, $CuGaO_2$, $CuCrO_2$ and $AgCrO_2$ show promising properties as dye-sensitized solar cells (DSSCs) because of their p-type conductivity.[3]

Delafossite is an ABO_2 structure with a transition metal at the A site and a transition or post-transition metal at the B site. This study will only present delafossite structures with Cu at A site, and Cr or Fe on B site. Delafossite is a layered structure, with a Cu and a Cr/Fe layer, where oxygens are octahedrally coordinated around Cr/Fe. Cu is linear coordinated to two oxygens, Cu having an oxygen directly above and below it in the c-axis. It can exist in two different space groups R-3mH, trigonal, or P63/mmc, hexagonal. R-3mH has two additional Cu layer in the unit cell. Both unit cells are shown in Figure 1, A) R-3mH and B) P63/mmc.

To obtain pure delafossite compound phases, hydrothermal reactions at temperatures between 70°C-700°C are needed, depending on the metals on the A and B sites. Hydrothermal synthesis of phase pure $CuCrO_2$ or $CuFeO_2$ have been reported.[1, 5] $CuCrO_2$ form the R-3mH polymorph as nanocrystals at 240°C, and $CuFeO_2$ form both polymorphs but as bulk phase at 70°C.[5, 6]

This study will focus on the synthesis and characterization of $CuCrO_2$ nanoparticles through Rietveld refinement and PDF analysis, and will illustrate the difficulties in modelling highly anisotropic and disordered materials. Several approaches will be carried out trying to describe the structural composition of the delafossite crystallites.

Delafossite polymorphs

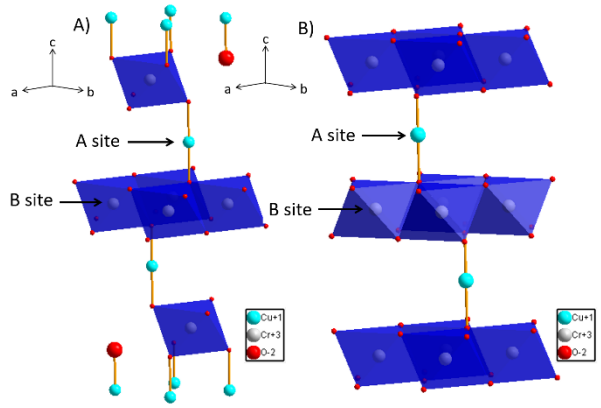

Figure 1. A) The R-3mH polymorph. Sides a = b = 2.974Å and c = 17.1Å. Angles α = β = 90° and γ = 120°. B) The P63/mmc polymorph. Sides a = b = 2.974Å and c = 11.4Å. Angles α = β = 90° and γ = 120°.

Multiple articles state different oxidation states for the same structures. A site stated as either +1 or +2 and B site +3 or +2.[4, 5] A proposal for a reaction mechanism and oxidation states of the metals will be stated, through considerations of the electrochemistry by Pourbaix analysis. See supporting information about Pourbaix diagrams. The synthesis and final product of $CuCrO_2$ will furthermore be compared to the one of $CuFeO_2$.

Theory

XRD and Rietveld Refinement

In a classical powder diffraction sample, a powder of small crystalline particles, all with random orientation, is radiated with a monochromatic X-ray beam. This beam, due to the periodic structural order of the crystal, is diffracted and a characteristic dataset is collected for that specific compound.

A diffraction peak arises when the X-ray beam interferes constructively with itself after diffraction, as described by Bragg.

$$2d \cdot \sin(\theta) = n \cdot \lambda$$

The distance between the planes, d, is measured with a wave having the wavelength λ. The angle between the incoming wave and the plane being θ. Data points are collected as intensities changing as a function of θ. Distances between the planes are related to the angle θ as seen in Bragg law. By relating distances within the unit cell to the angle, unique characteristics of a crystallite can be described with Bragg law, each crystallite having a unique diffraction pattern.

The intensity of a Bragg peak is proportional to the squared norm of the structure factor, $I \propto |F|^2$. The structure factor is given by the eq.

$$F = \sum_{i=1}^{Atom} f_i \cdot \exp\left(-B_i \cdot \frac{sin^2(\theta_h)}{\lambda^2}\right) \cdot \exp\left(2\pi i \vec{h} \vec{x_i}\right)$$

The structure factor sums over all atoms within the unit cell. X-ray scatters on electrons, and electron rich atoms scatter more as expressed by the atomic form factor, f_i. B_i is the Debye-Waller displacement factor. $\vec{h}$ is the Miller-indices for the reflection and $\vec{x_i}$ is the fractional coordinates for an atom within the unit cell.

Two things can cause broadening of Bragg peaks, either the instrument or the sample. Instrumental broadening arises from e.g. beam divergence and a spread in X-ray wavelength. Sample broadening is divided into two categories, strain and size broadening.

A crystal is described through an infinite translation of its unit cell, which gives rise to sharp Bragg peaks. Perfect crystals larger than c. 1μm can be described through an infinite translation of the unit cell. This is no longer the case working with nanocrystals, since the particles are only a few unit cell large. Scherrer eq. can through the width of the peaks estimate a size of the average crystallite.

$$D = \frac{K \cdot \lambda}{FWHM \cdot \cos(\theta)}$$

D being crystallite size, K shape factor, often set to 0.94, λ the wavelength of the incoming beam, full width at half maximum of a Bragg peak(FWHM) and the angle of the incoming beam, θ.

Strain broadening is caused by distortions in the crystal lattice. This results in different distances between two planes and thereby causes broadening. Bragg peak strain broadening varies proportional with tan(θ) and causes the effect to increase at higher angles. Strain and size broadening is weighted differently as a function of the scattering angle. Through the divergence in dependency of the angle the two can be distinguished from one another.

Rietveld refinement is a method where all the above, and much more, is taken into account when refining different parameters to fit a model to a dataset.[7] Different models can be used to describe the crystallites strain and size broadening, modelling the crystal as isotropic, a linear combination of symmetrized spherical harmonics(Popa-rules)[8] or an anisotropic "no rule model" where a combination of six vectors are used to describe the particle shape.

The Popa rule method describes the crystallites dimensions through an average of radius' starting from a sphere or an ellipsoid. A linear combination of symmetric harmonic functions is then refined to adjust the final shape of the particle. Each function depending on the Laue group of the crystal and anisotropy. More information about Popa-rules and anisotropic "no rule model" can be found in the supporting information.

Total Scattering and PDF

To make a PDF analysis, high Q space synchrotron data is needed, this requires a monochromatic high flux X-ray beam. Q space data can be Fourier transformed to gain structural information in real space. A broader spectrum of structural information is obtainable through PDF compared to Rietveld. An advantage of PDF is furthermore that the data allows separate analysis of local and global structural order.[9] By analysing the PDF under e.g. 10Å, it is possible to describe the local structure, and above 10Å the global structure. Deviations in model compared to measured data can be translated to errors in either the local or global structure.

I(Q) is the raw collected data. I(Q) contains both structural information, incoherent Compton scattering, scattering from the capillary etc. I(Q) is then corrected and normalized into the

structure function.

$$S(Q) = \frac{I(Q) - \langle f(Q)^2 \rangle + \langle f(Q) \rangle^2}{\langle f(Q) \rangle^2}$$

f(Q) being the form factor. S(Q) is the structure function. Because of the Debye-Waller factor the intensities die out with increasing Q. To get higher intensities at high Q, S(Q) is converted into F(Q).

$$F(Q) = Q[S(Q) - 1]$$

F(Q) is the reduced structure function which oscillates around zero and approach it with increasing Q. F(Q) is a function in reciprocal space but through Fourier transformation, it can be translated into real space distances, G(r).

$$G(r) = \frac{2}{\pi} \int_0^\infty F(Q) \sin(Qr)\, dQ$$

G(r) is directly comparable to real space due to its R(r) dependence.

$$G(r) = \frac{R(r)}{r} - 4\pi\rho_0$$

R(r) is the radial distribution function and real space distances, r is distances between atom within the sample and ρ_0 is the average number density of atoms.[10] Each peak indicates a distribution of distances within the sample. The formula for R(r) is.

$$R(r) = \sum_v \sum_\mu \frac{b_v b_\mu}{\langle b \rangle^2} \delta(r - r_{v\mu})$$

R(r) is described through a series of delta functions, $\delta(r - r_{v\mu})$. $r_{v\mu}$ is the magnitude of the separation of the atoms. The formula summing over all atoms, u and μ. The scattering factor of v and μ is multiplied and then divided with the squared mean scattering factor. $r_{v\mu}$ is the magnitude of the separation of the atoms.[10,11,12]

Experimental methods

Syntheses of $CuCrO_2$

The synthesis applied is based on the work by Xiong et al.[1] All chemicals were of >98% purity and was used without any further purification. 0.76g $Cu(NO_3)_2 \cdot 3H_2O$, 1.23g $Cr(NO_3)_3 \cdot 9H_2O$ and 0.71g NaOH were mixed into a total volume of 10ml using demineralized water as solvent. NaOH was used as a mineralizer and to increase the pH of the solution. The resulting suspension was stirred for about 20 minutes or until all powder was completely dissolved. The black/dark green solution was put into a 25ml Teflon-lined stainless steel autoclave. The autoclave was afterwards put into a preheated oven at 180-240°C for 24-120h. After heating, the autoclave was cooled for 1-2h at room temperature. The black precipitate was then washed 3 times with demineralized water, by centrifugation at 4500 rpm for 5-8minuttes. After centrifugation a black precipitate was seen in a yellow solution, and was washed until only a clear liquid plus the black precipitate was left. The final product was then dried for about 2 days in a fume hood.

All syntheses for $CuCrO_2$ delafossite and their different parameters can be seen in Table 1.

Table 1. $CrCuO_2$ experiments.

Experiment	Time [h]	Temperature [°C]
1	72	180
2	72	200
3	72	220
4	72	240
5	24	240
6	48	240
7	96	240
8	120	240

Parameter used in the synthesis making $CuCrO_2$. All syntheses are constant in NaOH and metal source concentration.

Syntheses of $CuFeO_2$

The synthesis applied is based on the work by John et al.[6] All chemicals were of >98% purity and was used without any further purification. 0.6g of $CuSO_4 \cdot 5H_2O$ was mixed with 15ml demineralized water in a 50ml Teflon-lined during magnetic stirring and heated to 70°C. After heating 0.66g of $Fe(SO_4) \cdot 7H_2O$ was added to the solution while kept at 70°C. When all powder was dissolved NaOH was slowly added until a pH of 11 was reached. While adding NaOH the temperature was measured to make sure it did not deviate more than a few degrees Celsius from 70°C. To determine the pH of the solution pH-paper was used. Afterwards the Teflon-lined was sealed in a stainless steel autoclave and put into a preheated oven at 70 °C. The solution was heated for 24h and the precipitate was washed and dried just as for CuCrO2.

XRD

XRD data were collected using a Bragg–Brentano setup using a $CuK_{\alpha 1}$(1.54Å) source on a BRUKER D8 Discover and a LYNXEYE detector. The CuK_α wavelength corresponds to the excitation energy for Fe causing it to fluoresce. The fluorescence will add background noise, and when obtaining data from the $CuFeO_2$ the lower and upper energy discriminators of the detector are therefore narrowed from 0.11V-0.25V to 0.19V-0.27V. All data were collected from 5-90θ with a step size of 0.005h and collected for 5h. To absorb the CuK_β radiation a nickel filter was used.

PDF

All PDF data were collected at Deutsches Elektronen-Synchrotron(DESY), beamline P02.1. The x-ray wavelength was determined to be 0.20717Å. CeO_2 was used as standard. All measurements were done at room temperature and all samples were loaded in 1mm kapton capillaries. A 2D Perkin-Elmer amorphous silicon detector were used.

Results and Discussion

$CuCrO_2$ synthesis and characterization

Figure 2 shows the PXRD data obtained for the $CuCrO_2$ samples. The data sets show both sharp and broad peaks. The sharps peaks indicating the presence of highly crystalline particles. These peaks can be assigned to CuO. While the broad peaks can be assigned to the delafossite structure in space group R-3mH. Two sets of syntheses were made, one changing the temperature and

one varying time heated.

At Figure 2 A) only one of the dataset have no sharp peaks, this indicating the absence of the CuO phase. The data from samples synthesized at 24h, 48h, 96h and 120h looks remarkably similar. It would appear that forming $CuCrO_2$ and CuO at these temperatures are equally favourable. The CuO phase simply disappear at 72h. This indicates how dependent $CuCrO_2$ nanocrystals are of the chemical environment. The sample at 72h have been reproduced to verify the absence of CuO. If the heating is continued beyond 72h the CuO phase reappears.

B) shows a clear change in the ratio between the two phases. At 180°C the intensities between the CuO and $CuCrO_2$ phases are large. This is seen by comparing the sharp CuO peaks with the broad $CuCrO_2$ peaks. As the temperature increases the ratio between the $CuCrO_2$ and CuO phase change. This indicates that an increase in temperature makes the delafossite formation more favourable than CuO.

In both A) and B) there are only indications of one of the two polymorphs of $CuCrO_2$, namely the R-3mH polymorph. This does not agree with the results of Xiong et al[1] who obtained both polymorphs at 240°C heated for 60h, while PXRD from this article only indicates the presence of the P63/mmc polymorph.

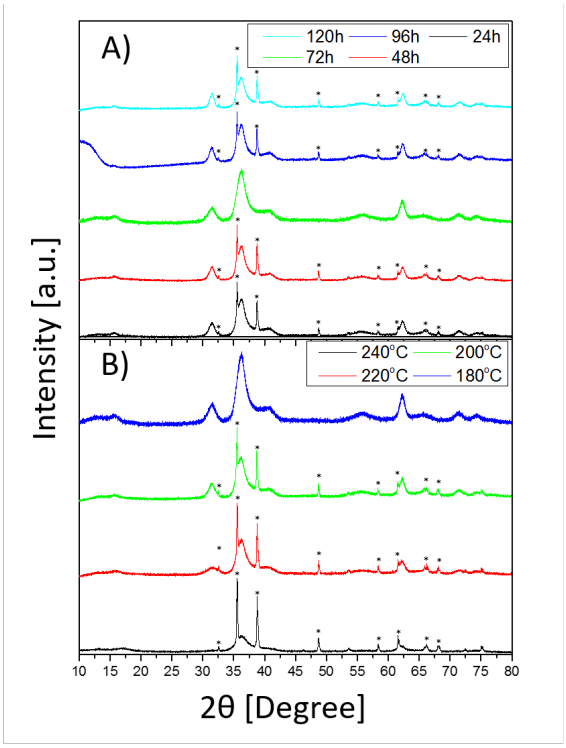

PXRD-data, time and temperature

Figure 2. A) shows PXRD data from the samples varying in time. The one obtained at 96h has a broad peak at low angle caused be bad calibration of the instrument. B) shows PXRD data from syntheses at different temperatures. Indication of CuO as marked with *.

To obtain more structural information about the pure delafossite phase, synthesised for 72h at 240°C, multiple Rietveld refinements were made. First an isotropic model assuming spherical crystallite sizes was fitted to the data from the $CuCrO_2$ nanoparticles. As seen in Figure 3 A) multiple peaks are not well describe through this model, [0 1 4], [0 1 8] and [0 0 12] reflections. The model furthermore does not describe the peak broadening. This indicates that the broadening cannot be described through an isotropic model, therefore the intensities of the peaks are increased trying to fit the broadening. by modelling the particles as a sphere too much intensity is obtained. The [1 1 0] indicates the exact opposite since the intensity is lower than measured. This could indicate presence of anisotropic particles and is therefore not able to fit all peak intensities. All peak having to high intensity is a reflection having a high l value compared to h and k. By modelling a crystallite being shortened at the l direction, the intensities will drop at these reflections. This corresponds to the [1 1 0] being too low in intensity. By prolonging the crystallite in the h and k directions the intensity of the peak will amplify. Broadening of the peaks causes the intensities to be spread over larger angles, and thereby decreasing the height of the peaks.

B) Is modelled using Popa-rules. With Popa-rules a linear combination of symmetrized spherical harmonics is refined trying to describe the particle size and shape. By describing the particle shape with four parameters the fit has improved significantly. Popa rules are described further in supporting information. The [0 1 4], [0 1 8] and [1 1 0] reflection now match the intensities of the measured data. Only the fit of the [0 1 8] reflection seem to have deteriorated. Figure 4 shows the particle shape modelled with Popa-rules. The modelled particle shape is highly unphysical, but it helps indicating a possible average shape for the particles. The most likely shape for $CuCrO_2$ to form would be platelets. The idea that $CuCrO_2$ crystalizes as platelets match the deviation in peak broadening when using an isotropic model. A better fit is possible by adding more parameters in the Popa-rules. This would also change the shape of the average crystallite and quite possible make an even more unphysical shape.

To get a more physical crystallite shape anisotropic “no rule refinement” was used. The refinement is shown in Figure 3 C). To model the platelet, the size along three vectors were refined, 11, 22 and 33 vector. The 11 and 22 vectors are formed by translation of the trigonal unit cell along the a and b axis, see Figure 1. The 11 and 22 vector forms the plane of the platelet and 33 the size along c, i.e. gives information about the number of layers stacked. The sizes along 11 and 22 are set to be equal each other, as a and b are equal in the trigonal unit cell.

Rietveld refinements of pure $CuCrO_2$

Figure 3. A) Is modelled as isotropic spherical particles. B) Is modelled with Popa-rules and C) with anisotropic "no rules model". Above each peak the reflection is written.

The largest difference in using the Popa-rules model and the anisotropy no rules model is the intensity of the [0 1 8]. While using Popa-rules the intensity of the [0 1 8] reflection is not fitted.

$CuCrO_2$ is a layered structure and translation along the a and b direction would form a platelet. Distortion between the layers could cause the thickness of the platelet to differ causing strain broadening.

Table 2. Weighted R-factor

Model	R_{wp} [%]
Isotropic, spherical	5.3284
Popa-rules	4.4448
Anisotropic no rules, platelet	4.3889

The table compares different models R_{wp} values.

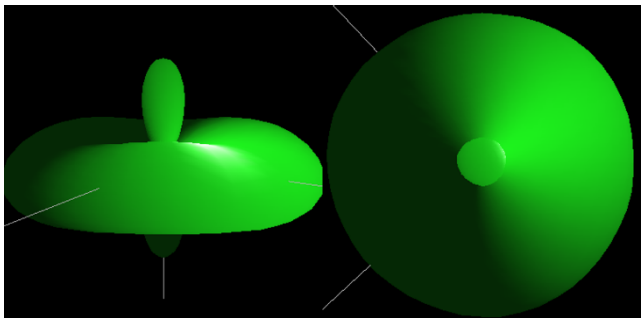

Popa-rules particle model

Figure 4. Shows a model of the particle obtained through Popa-rules. The model is platelet shaped in the x-y plane but have a p-orbital shape along the z-axis.

All models described above are fitting the [0 0 6] reflection width, intensity and position, but all are having problems fitting the [0 0 3] reflection at lower 2θ values. This indicates that the large anisotropy of the particles means that conventional Scherrer analysis cannot be used. Applying Scherrers several assumptions were made, one of them being that a crystal can be described as a sphere. Making Rietveld refinement on nanoparticles makes the infinite translation assumption invalid, and the correlation between the broadening of the peaks and the size of the crystallite unable to be described by Scherrers eq.[13]

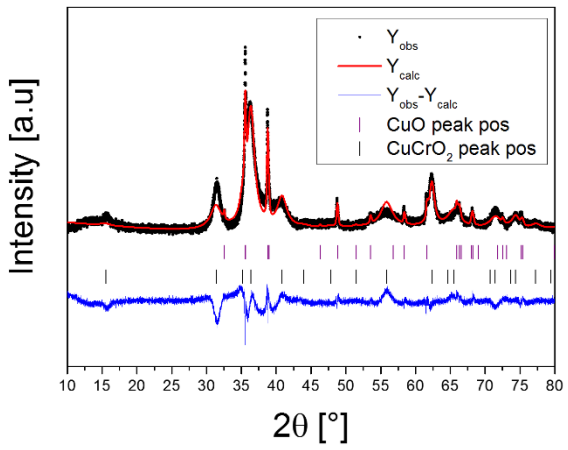

Rietveld refinement on multiple phases

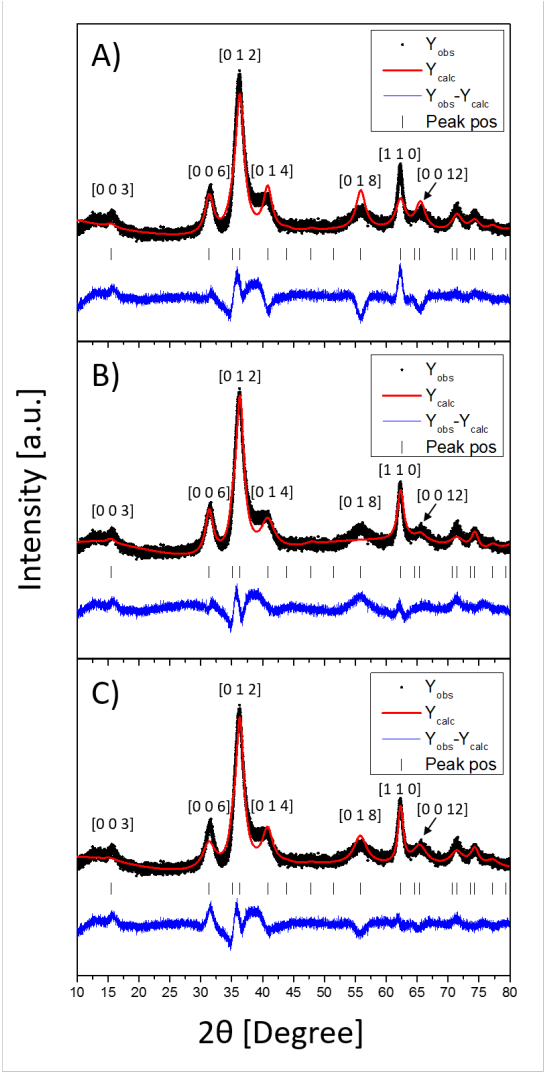

Figure 5. Rietveld refinement of multiple phases on 24h.

To get a better understanding on how the change in parameters affect the final product, Rietveld refinements of the $CuCrO_2$ and CuO phase were made. CuO being modelled as isotropic crystallites. All data, shown in Figure 2, have been refined and through Rietveld refinement sizes and phase ratios were obtained. Refinements for $CuCrO_2$ were done using anisotropic "no rule" model. Figure 6 shows the changes in size and ratio between the phases. The crystallite size along a and c only varies about 2nm no matter the synthesis parameters. The only outlier is 96h, this could be caused by the bad data. The sizes obtained through Rietveld refinement is only an average of the scattering crystallite, and not the definite particle size. It is therefore not possible to conclusive say anything about the whole particle, but only the crystalline part of it. Other methods have to be used to determine the definite size of the particle e.g. transmission electron microscopy(TEM).

Figure 6 C) and D) show the ratio between the two phases. When having time as varying parameter, all samples except 72h have a CuO/$CuCrO_2$ ratio about 1:1. It is interesting to notice that the ratio almost does not change from 24h to 48h, but from 48h to

72h the delafossite structure is so favourable that no CuO is synthesized. Further increase in time shifts this equilibrium back to a 1:1 ratio between the phases. In some extent D) shows the same tendency. Increasing the temperature by 20°C changes the percentage between the phases with approximately 2%. This continuously happens until 240°C. Here the equilibrium gets pushed sufficiently in favour of $CuCrO_2$ and the product is 100% delafossite. The synthesis producing pure $CuCrO_2$ have been reproduced.

Phase ratio and size distribution

Figure 6. A) and B) showing the sizes along A and B in nm. C) and D) shows the percentage of the two phases present. A) and C) being the syntheses with time as changing parameter, B) and D) temperature. Data is received through anisotropic no rules model.

To understand why the gap of synthesizing $CuCrO_2$ delafossite is so narrow a further analysis at the reaction must be done. In older literature, the oxidation states of the metals (Cu and Cr) in the delafossite structure are only vaguely described. Both Cu(II) with Cr(II) or Cu(I) with Cr(III) are being used.[14] Previous studies have shown that $CuCrO_2$ only forms at elevated pH value.[15] In the reaction used here, Cu(II) is added in the form of $Cu(NO_3)_2{\cdot}3H_2O$. The reaction is strongly pH dependent, if the pH is not high enough no delafossite is formed. This could indicate that Cu(II) needs to be reduced to Cu(I) for the reaction to take place, as this will only happen at high pH values. This is supported by the Pourbaix diagram for Cu, which can be found in supporting information. When looking at the diagram it is seen that the region where Cu(I) is stable is very narrow. Comparing the Pourbaix diagram for Cr and Cu, it shows that the zones where Cu(I) and Cr(III) are stable overlap. Pourbaix diagram for Cr can be found in supporting information.

The stability of the Cr^{3+} ion can be understood through metal-ligand interactions. Cr is coordinated octahedrally to oxygen. All of Cr ligands feel the same environment so they bind equally strong to Cr. This is supported both by the crystallography file and others research for $CuCrO_2$.[2, 16] This conformation makes the classic octahedral orbital splitting, having three orbitals being equally low in energy and two equally high in energy. Cr(III) is especially favourable in octahedral conformation since it can put one electron into each of the low energy levelled orbitals. This leaves a big energy gap between HOMO and LUMO. Each orbital is coordinated perpendicular to each other, causing the electrons to not repel each other. Oxygen coordinates to three Cr and one Cu, while Cu coordinates to two oxygens. Oxygen having a coordination number of 4 and -2 charge making oxygen share 0.5 electron density into each orbital it coordinates with.

PDF on $CuCrO_2$

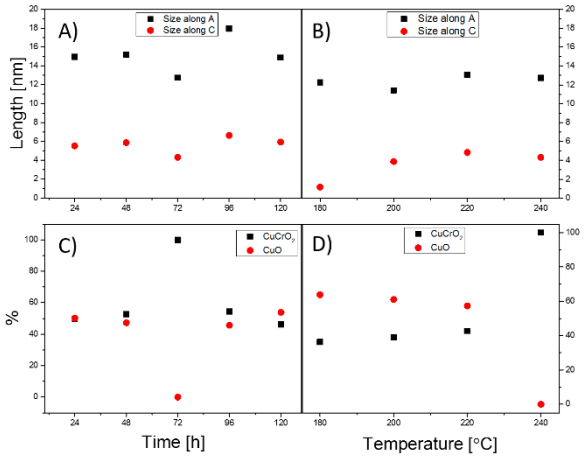

Several Rietveld refinements were carried out trying to describe the crystal structure and morphology of $CuCrO_2$. None of the models were able to make a fit describing all peak positions, widths and intensities. To obtain additionally structural information about the crystallites, PDF analysis was applied. Each peak within the PDF analysis can be directly assigned to interatomic distances within the sample.

PDF data

Figure 7. A) Model of $CuCrO_2$ fitted to local structure, 0.5-10Å value and B) fit from 0.5-19Å. 1) Indicating the metal oxygen distance. 2) Is the Cr-Cr distance. 3) Cu-Cr distance 4) Cr-O distance 5) Cu-O distance 6) Cu-Cu or Cr-Cr distance in another layer of the structure.

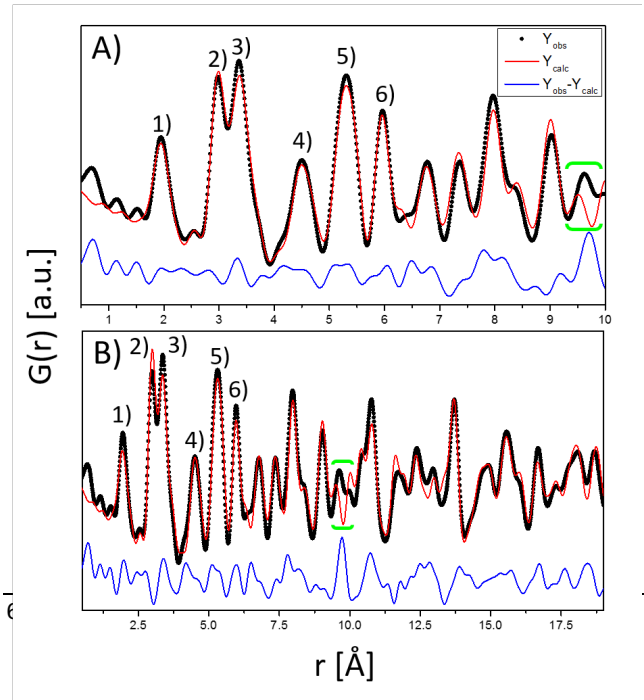

Two refinements of $CuCrO_2$ were made. One only fitting the local structure 0.5-10Å, and one fitting the global structure 0.5-19Å. Figure 7 shows both fit of the local and global structure. Figure 7 A) shows a fit which almost matches at all peak positions and intensities. At 6Å the intensities start deviating a bit but the positions still match. Peak 1) are the metal oxygen distances, Cr-O distance shown in Figure 8 A) and the Cu-O distance can be seen in Figure 1. Peak 2) is the Cr-Cr distance between octahedral sharing an edge, which is shown in Figure 8 B). Peak 3) is the distance between Cu to the nearest Cr. Peak 4) is the Cr-O shown in Figure 8 D). Peak 5) corresponds to the Cu-O distance and is visualized at Figure 8 C) as the 5.34Å distance. Peak 6) is either Cr-Cr or Cu-Cu distance between the layers. All these peaks are well described by the chosen structure.

Figure 7 B) is the same model but fitted to longer range data. As the model is fitted to higher r the R_{wp} rises. This could be due to faults in the structure, since high r value describe distances between unit cells and no longer only within them. Stacking fault then causes periodic distances between unit cells to deviate from the model used. The model is trying to describe the long range

order, which may contain stacking faults. Stacking faults then forces the unit cell to change trying to describe the global structure. By only fitting below e.g. 10Å the local structure can be determined, depending on the unit cell. This consequence is clear when looking at the 2) peaks as it gain an intensity increase. The loss or increase in intensities could also be due to Cu or Cr atoms coordinating at the wrong site, because the scatter differently from each other. Trying to describe the stacking faults

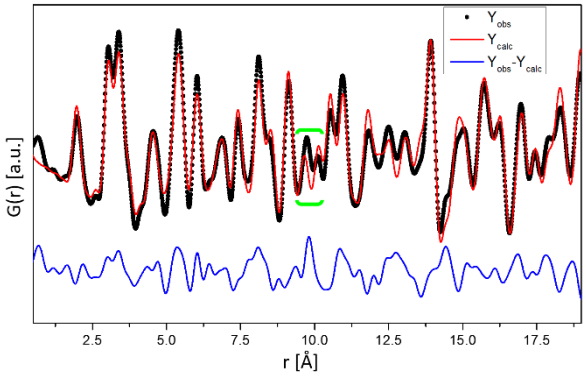

all atoms were refined to have a separate displacement factor along the c axis. This gave a small decrease in the R_{wp}.

Distances within the unit cell

Figure 8. A) Distance from Cr to its oxygen ligands. B) Cr-Cr distance between to octahedra sharing an edge. C) Shows the distance from Cu to the nearest oxygen layer. An oxygen being directly beneath the Cu. D) The distance from Cr to oxygen in the neighbouring octahedra.

A green area is marked on Figure 7 both on A) and B). This distance is not within the model for the R-3mH delafossite structure. This peak could be caused by stacking faults or by both structural polymorph being present in the sample. In fact, the P63/mmc polymorph describes the marked distance, few distances differ between the two polymorphs, making it hard to separate them from each other. The separation of the two polymorphs become even harder when analysing anisotropic nanocrystals, the broadening causing the peaks to have a large

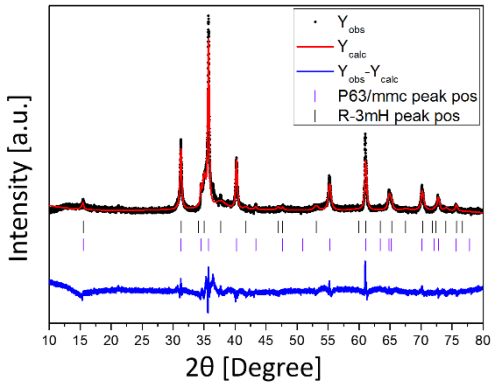

overlap with adjacent peaks. The platelets could be a stacked structure of the two polymorphs, with the R-3mH being the dominating one. The P63/mmc cannot describe the locale structure as well as the R-3mH polymorph. This could indicate that only a small amount of P63/mmc is formed.

Discussion on Rietveld and PDF $CuFeO_2$

The synthesis of $CuFeO_2$ were made three times to show reproducibility of final product. All three PXRD data sets are indicating that the same phases are present, therefore only one were analysed further. The PXRD data can be found in the supporting information.

Rietveld of $CuFeO_2$

Figure 9. The Popa rule model were used to describe the shape of the particles size and ratio between the of the two polymorphs.

To characterize the structure Rietveld refinement were used. Isotropic, Popa rules and anisotropic "no rules" were used to describe the synthesized compounds. Refined parameters for all three models are found in supporting information. PXRD data for $CuFeO_2$ R-3mH polymorph was not obtainable at ICSD. To make a characterization of the structure the model for $CuCrO_2$ was modified. Cr was exchanged with Fe, since they scatter differently, and the dimensions of the unit cell was changed to match the ones for $CuFeO_2$.

PDF analysis of $CuFeO_2$

Figure 10. PDF analysis of $CuFeO_2$. PDF data is only fitted with the R-3mH polymorph. Same undescribed peak for $CuCrO_2$ occur for $CuFeO_2$ and is marked with green.

Figure 9 showing the Rietveld refinement of $CuFeO_2$. The refinement indicating the presence of both polymorphs in a 1:1

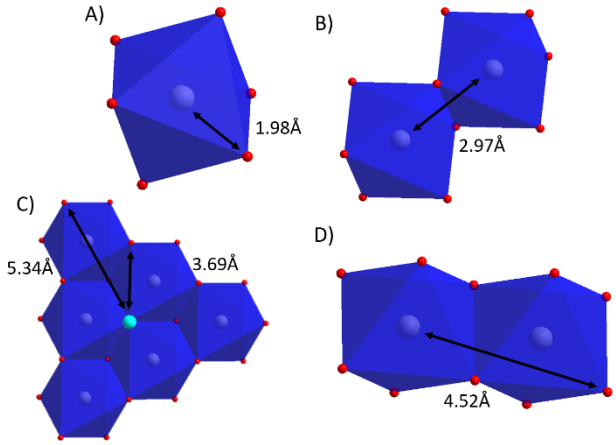

ratio. Popa rules indicating that the crystallite described from the R-3mH polymorph form platelets and the P63/mmc as spheres. Pictures can be found in supporting information. It is possible that two different crystallites are formed, one being described through the R-3mH polymorph as platelets, and the other by the P63/mmc polymorph as isotropic. One could imagine the two polymorphs stacking on top of another along c, but holding the symmetry along a and b while translate. More complicated mixtures of the polymorphs could also be a solution.

To get further structural information PDF is used. PDF analysis supports the Rietveld refinement, showing that $CuFeO_2$ has been synthesized, as seen in Figure 10. All peak positions and most intensities match. The same peak at 9.6Å is poorly described as for $CuCrO_2$. The R-3mH polymorph gave the best fit, despite of the Rietveld refinement indicating the presence of both polymorphs. Despite the $CuFeO_2$ particles being larger than the one of $CuCrO_2$, the PDF indicate the same stacking faults.

Conclusion

The delafossite crystallite size is extremely dependent on which metal occupies the A and B site. Having Cu located at A site then forces the synthesis to be done at high pH values. Cu(II) has to be reduced to Cu(I) before the delafossite structure can form. Changing the B site from Cr to Fe causes the crystallites size to differ.

Through multiple Rietveld refinements of $CuCrO_2$ the particles were determined to form nanoplatelets described by the R-3mH polymorph. Rietveld refinements only indicate one of the two polymorphs being present within the samples. Through PDF the local structure was determined, but the global structure could not be completely understood. PDF showed one distance which the R-3mH polymorph could not describe, but further analysis showed that the P63/mmc polymorph could describe it. This indicates that the P63/mmc polymorph might be present within the samples. Several guesses were made trying to describe the global structure. Whether the crystallites contain both polymorphs or different types of crystallites are present, are yet to be determined. Both PDF and Rietveld indicates that stacking faults or defect are present within the nanoparticles.

Rietveld refinement and PDF analysis reveals the presence of both $CuFeO_2$ polymorphs in the sample. $CuFeO_2$ have been proven possible to synthesize at 70°C. Despite $CuFeO_2$ being larger than $CuCrO_2$ indications of similar stacking faults are visible.

For further studies X-ray absorption near edge structure(XANES) should be tested to identify the metals oxidation states. To check the size of the particles and see if they are concealed by an amorphous layer TEM can be used. By using TEM the shape of the particles could be verified and thereby see if the crystallites are anisotropic.

Acknowledgements

Special thanks to the people who have worked so hard getting me through this project. My supervisor Kirsten M.Ø Jensen adjunct at the Nanoscience Center and Department of Chemistry, University of Copenhagen, for being an outstanding supervisor who always makes time to guide and give constructive feedback. A Supervisor who always have a new idea or adjustment to improve the project. Troels Lindahl Christiansen Ph.D student at the Nanoscience Center and Department of Chemistry, University of Copenhagen, for always being there to answer questions about anything, no matter how stupid it should be. Mikkel Juelsholt master student at the Nanoscience Center and Department of Chemistry, University of Copenhagen, for helping me with different types of Rietveld refinements in Maud and PDF analysis. Emil Rössing Elholm master student at the Nanoscience Center and Department of Chemistry, University of Copenhagen, for always wanting to discuss my data and refinements with me. Patrick Nawrocki bachelor student at the Nanoscience Center and Department of Chemistry, University of Copenhagen, for bringing me coffee in the direst of moments.

Notes and references

1. D. H. Xiong, Z. Xu, X. W. Zeng, W. J. Zhang, W. Chen, X. B. Xu, M. K. Wang and Y. B. Cheng, *J. Mater. Chem.*, 2012, **22**, 24760-24768.
2. I. C. Kaya, M. A. Sevindik and H. Akyildiz, *J. Mater. Sci.-Mater. Electron.*, 2016, **27**, 2404-2411.
3. D. H. Xiong, Q. Q. Zhang, S. K. Verma, H. Li, W. Chen and X. J. Zhao, *J. Alloy. Compd.*, 2016, **662**, 374-380.
4. H. N. Abdelhamid, S. Kumaran and H. F. Wu, *RSC Adv.*, 2016, **6**, 97629-97635.
5. M. John, S. Heuss-Assbichler, S. H. Park, A. Ullrich, G. Benka, N. Petersen, D. Rettenwander and S. R. Horn, *J. Solid State Chem.*, 2016, **233**, 390-396.
6. M. John, S. Heuss-Assbichler and A. Ullrich, *J. Solid State Chem.*, 2016, **234**, 55-62.
7. R. A. Young, *The Rietveld Method*, Oxford University Press, 1995.
8. N. Popa, *Journal of Applied Crystallography*, 1998, **31**, 176-180.
9. G. Paglia, E. S. Bozin and S. J. L. Billinge, *Chem. Mat.*, 2006, **18**, 3242-3248.
10. T. Egami, Billinge, S. J. L., *Underneath The Bragg Peaks*, 2003, **Second volume**.
11. P. Juhas, T. Davis, C. L. Farrow and S. J. L. Billinge, *Journal of Applied Crystallography*, 2013, **46**, 560-566.
12. S. J. L. Billinge, in *Uniting Electron Crystallography and Powder Diffraction*, eds. U. Kolb, K. Shankland, L. Meshi, A. Avilov and W. I. F. David, Springer Netherlands, Dordrecht, 2012, DOI: 10.1007/978-94-007-5580-2_17, pp. 183-193.
13. J. Baruchel, *Neutron and synchrotron radiation for condensed matter studies*, Springer-Verlag, 1993.
14. W. Dannhauser and P. A. Vaughan, *Journal of the American Chemical Society*, 1955, **77**, 896-897.
15. B. J. Ingram, G. B. Gonzalez, T. O. Mason, D. Y. Shahriari, A. Barnabe, D. G. Ko and K. R. Poeppelmeier, *Chem. Mat.*, 2004, **16**, 5616-5622.
16. T. N. M. Ngo, T. T. M. Palstra and G. R. Blake, *RSC Adv.*, 2016, **6**, 91171-91178.